STATISTICS, OPTIMIZATION AND INFORMATION COMPUTING
Stat., Optim. Inf. Comput., Vol. **x**, Month 202x, pp 0–24.
Published online in International Academic Press (www.IAPress.org)

Comparative Control of PWM-CSCs in Single-Phase Microgrids with Sinusoidal Injection

Angélica Mercedes Nivia-Vargas [1], Oscar Danilo Montoya [2,*], Walter Gil-González [3]

[1] *Doctoral student in Engineering, Universidad Distrital Francisco José de Caldas, Bogotá, Colombia*
[2] *Faculty of Engineering, Universidad Distrital Francisco José de Caldas, Bogotá, Colombia*
[3] *Department of Electrical Engineering, Universidad Tecnológica de Pereira, Colombia*

Abstract This paper deals with the issue of control strategies for pulse-width modulation current-source converters, as they play a crucial role in integrating renewable energy sources and managing variable loads in modern power systems. A comparative analysis is carried out between a nonlinear proportional-integral (PI) controller and two passivity-based approaches, *i.e.*, interconnection and damping assignment passivity-based control (PBC) and PI-PBC. This analysis aims to evaluate the dynamic response, robustness, and stability of each method under realistic operating conditions. Simulation results reveal that, while PI-based controllers perform satisfactorily under steady-state or slowly varying conditions, their performance deteriorates significantly in the face of abrupt load changes or transient disturbances. In contrast, passivity-based strategies demonstrate superior robustness, enhanced disturbance rejection, and improved system stability across a wide range of scenarios. Comprehensive simulations were conducted under variable load profiles, including step and ramp disturbances, in order to assess control performance through key metrics such as current tracking accuracy, total harmonic distortion, and settling time. The results provide valuable insights for designing reliable and adaptive control schemes in applications involving microgrids, electric drives, and energy conversion systems.

Keywords Variable Load Control, Stability, Harmonic Distortion, Nonlinear Dynamic Systems, Switch-Mode Power Conversion

DOI: 10.19139/soic-2310-5070-2692

Nomenclature

Acronyms

FLC Fuzzy logic control

IAE Integral of the absolute error

IDA-PBC Interconnection and damping assignment passivity-based control

IGBT Insulated gate bipolar transistors

ISE Integral of the squared error

ITAE Integral of the time-weighted absolute error

ITSE Integral of the time-weighted squared error

*Correspondence to: O. D. Montoya (Email: odmontoyag@udistrital.edu.co). Faculty of Engineering, Universidad Distrital Francisco José de Caldas, Bogotá, Colombia

ISSN 2310-5070 (online) ISSN 2311-004X (print)

MOSFET Metal-oxide-semiconductor field-effect transistor

MPC Model predictive control

NPI nonlinear proportional-integral

PI Proportional-integral

PI-PBC Proportional-integral passivity-based control

PWM-CSC Pulse-width modulation current-source converter

PWM-VSC Voltage source converters

SMC Sliding mode control

THD Total harmonic distortion

Parameters

$\mathcal{D}$ Energy storage array

$\mathcal{J}$ Skew-symmetric interconnection matrix

$\mathcal{R}$ Dissipation matrix

$\mathcal{V}(x)$ Lyapunov function

$\tilde{x}_1$ Error of x_1

$\tilde{x}_2$ Error of x_2

$\tilde{x}_3$ Error of x_3

ϑ Vector of external inputs

C_o Capacitor value on the AC side (F)

k_i Integral constant

k_p Proportional constant

L_g Inductor value on the AC side (F)

L_s Inductor value on the DC side (H)

m Modulation index

R_g Linear load on the AC side (Ω)

r_s Series-modeled coil resistance on the DC side (Ω)

u Control signal

$u^\star$ Smooth control input for maintaining the system's desired behavior

V_s DC input voltage source (V)

x_1 State variable representing the current inductor on the DC side i_i (A)

x_2 State variable representing the voltage capacitor v_o (V)

x_3 State variable representing the current inductor on the AC side v_o (V)

$x_1^\star$ Desired operating point of x_1

$x_2^\star$ Desired operating point of x_2

$x_3^\star$ Desired operating point of x_3

1. Introduction

Power electronic converters play a crucial role in the efficient integration of renewable energy sources, energy storage systems, and variable loads within modern electrical networks [1]. In particular, pulse-width-modulation current-source converters (PWM-CSCs) are widely employed in applications where maintaining current stability is essential [2]. However, when these converters supply variable current loads (*e.g.*, in systems involving inductive components), designing robust control strategies becomes a significant challenge. In this context, it is essential to evaluate and compare the performance of different control approaches to ensure a reliable and stable operation under varying load conditions [3].

The study of control strategies for PWM-CSCs is of great relevance in both academia and industry. These converters are commonly utilized in scenarios that critically necessitate the injection of a regulated and sinusoidal current, as is the case with microgrids, electric drives, and renewable energy systems [4, 5]. Nevertheless, the presence of nonlinearities, switching dynamics, and variable loads poses considerable difficulties in achieving system stability and high performance [6]. While traditional linear controllers offer simplicity, they often lack the robustness required under dynamic conditions or abrupt load variations [7]. This has driven the exploration of advanced control techniques, particularly those rooted in nonlinear and passivity-based control (PBC) theory, which promise improved performance in terms of stability, disturbance rejection, and transient response.

Moreover, several alternative control methodologies have been investigated in recent years, in an attempt to enhance converter performance. Model predictive control (MPC), sliding mode control (SMC), and adaptive and backstepping techniques, as well as intelligent approaches such as those involving fuzzy logic and neural networks, have demonstrated potential in addressing nonlinearities, parameter variations, and real-time adaptability [8–12]. These efforts underscore the dynamic nature of this research field and the growing need for systematic comparative studies. A summary of relevant strategies and their application domains is presented in Table 1.

Table 1. Summary of converter control strategies in the recent literature

Control strategy	**Application**
Nonlinear proportional-integral (PI) control	Power electronics lab converter in single-phase [6]
PI-PBC	DC motor drive in single-phase [13]
Interconnection damping assignment (IDA) PBC	Grid-connected CSC in single-phase [14]
MPC	Renewable energy integration in three-phase [11]
SMC	Inductive load regulation in single-phase [10]
Adaptive control	Variable load conditions in three-phase [9]
Backstepping control	Industrial current regulation in three-phase [12]
Fuzzy logic control (FLC)	Smart grids in single-phase [8]

1.1. Contributions

This work contributes to the body of knowledge on PWM-CSC control by developing and analyzing three control strategies: a nonlinear proportional-integral (NPI) controller [6], a PI-PBC [13], and an IDA-PBC [14]. A comparative evaluation of these methods can provide insights into their relative strengths and limitations, particularly in the presence of load variability and switching dynamics.

The aforementioned controllers were designed based on energy-based modeling and Lyapunov stability theory, employing a Hamiltonian representation to exploit the system's passivity properties [15]. The PI-PBC introduces

additional damping mechanisms to enhance transient behavior, while the NPI controller is adapted to manage the converter's intrinsic nonlinear characteristics. IDA-PBC, in particular, leverages the system's structure through Hamilton-Jacobi theory, facilitating the formal assignment of desired dynamics.

The results of simulations carried out in MATLAB (version 2024b) helped to assess the controllers' effectiveness using key performance indicators such as settling time, overshoot, robustness to load changes, and harmonic distortion. This study lays the foundation for future control developments, such as hybrid schemes, integrations with MPC, and extensions to three-phase systems or smart grids. The possibility of incorporating artificial intelligence techniques for adaptive real-time control is also discussed as a future direction.

1.2. Document structure

This document is organized as follows. Section 2 presents the model of a single-phase PWM-CSC. Here, the operating principles of the converter are described, emphasizing the roles of current modulation and energy storage components. Next, a state-space model is developed for the operating trajectory, forming the basis for control design. Afterwards, the Hamiltonian model is derived, enabling the application of energy-based control strategies, particularly those grounded in passivity theory.

Section 3 is devoted to formulating and designing three control strategies. The first is an NPI controller that aims to improve the dynamic response by incorporating system nonlinearities, and the second is PI-PBC, which combines classical PI action with passivity-based concepts in order to enhance robustness and stability. The third strategy, IDA-PBC, leverages the system's Hamiltonian structure to achieve asymptotic stability via energy shaping and damping injection.

Section 4 compares the performance of these control strategies. The evaluation criteria include classical integral performance indices such as the integral of the squared error (ISE), the integral of the time-weighted squared error (ITSE), the integral of the absolute error (IAE), and the integral of the time-weighted absolute error (ITAE). These indices enable a quantitative assessment of control performance in terms of transient response and steady-state accuracy. Additionally, a total harmonic distortion (THD) analysis is performed to evaluate the quality of the output current waveform generated by each method.

The document concludes with Section 5, which summarizes the main findings and discusses potential directions for future research. These include extending the proposed control strategies to three-phase systems, integrating MPC and intelligent algorithms, and developing hybrid controllers to improve performance in complex and dynamic power electronic applications.

2. PWM-CSC converter modeling

PWM-CSCs constitute a key topology in applications requiring a stable and controlled output current, such as high-voltage alternating-current (AC) transmission systems, electric drives, and microgrids [16]. Their design enables output current regulation through PWM strategies, providing better control compared to other current converters. However, modeling these converters represents a challenge due to their nonlinear nature and the presence of inductive elements that affect their dynamics.

This section analyzes the operating principles of the single-phase PWM-CSC, considering its structure and fundamental operation [6]. Subsequently, its state-space mathematical modeling is developed, providing a representation that facilitates system analysis and controller design [7]. Both a model at the operating point/trajectory and a Hamiltonian formulation are proposed.

2.1. Operating principles of the PWM-CSC

As previously stated, PWM-CSCs are a key topology in energy conversion systems, particularly in applications requiring precise current regulation [17]. Unlike voltage source converters (*i.e.*, PWM-VSCs), PWM-CSCs incorporate an input-side inductor to maintain a continuous current flow, which makes them well-suited for applications involving inductive loads [18].

The operating principle of a PWM-CSC relies on the controlled switching of power semiconductor devices, such as IGBTs or MOSFETs, in order to regulate the current supplied to the load [6]. PWM enables the adjustment of both the magnitude and the waveform of the output current, effectively minimizing harmonics and enhancing the overall system efficiency [19]. Figure 1 depicts the circuit configuration of a PWM-CSC connected to an AC microgrid. The main control objective is to generate a sinusoidal current to be injected into the grid while maintaining a unitary power factor.

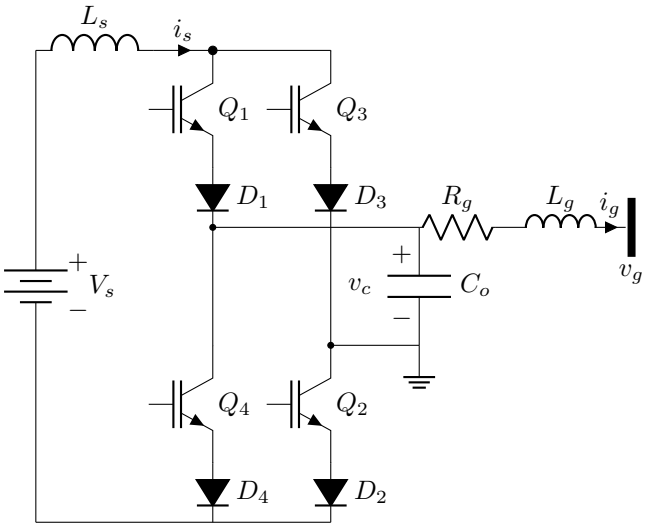

Figure 1. Configuration of the studied PWM-CSC

To facilitate the analysis and design of advanced control strategies, a time-domain mathematical model of the converter was developed. In this vein, a state-space representation was employed to capture the system's dynamic behavior.

Considering the primary function of the PWM-CSC as a current-regulating device, its dynamic model is derived from the circuit's underlying differential equations.

$$L_s \frac{di_s}{dt} = V_s - r_s i_s - m v_c, \tag{1}$$

$$C_o \frac{dv_c}{dt} = m i_s - i_g. \tag{2}$$

$$L_g \frac{di_g}{dt} = v_c - R_g i_g - v_g. \tag{3}$$

where L_s is the input inductance, i_s is the inductor current, V_s is the input voltage, r_s is the equivalent series resistance of L_s, m is the modulation index, V_c is the capacitor voltage, C_o is the output capacitor, i_g is the load current, R_g and L_g represent the load, and v_g is the microgrid voltage supplied by the converter.

In matrix form, and by defining the state variables as $x_1 = i_s$, $x_2 = v_c$, and $x_3 = i_g$, the system can be expressed as follows:

$$\begin{bmatrix} L_s \dot{x}_1 \\ C_o \dot{x}_2 \\ L_g \dot{x}_3 \end{bmatrix} = \begin{bmatrix} -r_s & -u & 0 \\ u & 0 & -1 \\ 0 & 1 & -R_g \end{bmatrix} \begin{bmatrix} x_1 \\ x_2 \\ x_3 \end{bmatrix} + \begin{bmatrix} V_s \\ 0 \\ -v_g \end{bmatrix} \tag{4}$$

with u being the control signal that modifies the modulation m.

Figure 2 presents a flow diagram of the correspondence between the physical components of the PWM-CSC. On the left, the key elements of the power stage are identified, including the DC voltage source V_s, the AC-side inductor L_g, the output capacitor C_o, and the load impedance represented by R_g and L_g.

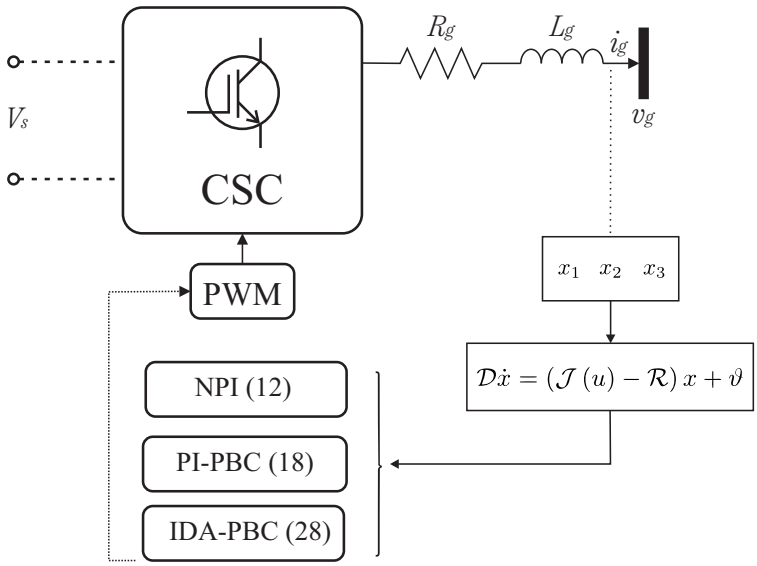

Figure 2. Relationship between the converter's physical components and its mathematical modeling

2.2. Model at the operating trajectory

To analyze and design control strategies for PWM-CSCs, it is essential to derive a simplified mathematical representation around a specific operating point or trajectory [20]. Given the nature of the system and its application in AC power conversion, the selected operating trajectory for $x_3^\star$ is a sinusoidal current defined as $I_g \sin(\omega t + \phi)$, where I_g is the amplitude of the desired current, ω is the angular frequency, and ϕ is the phase shift relative to a reference frame. This trajectory characterizes the steady-state behavior of the current signal and allows for small-signal linearization around it, which is necessary for the subsequent control design [21].

In grid-connected systems, the injection of a sinusoidal current synchronized in both frequency and phase with the grid voltage is imperative for ensuring power quality, minimizing harmonic injection, and maintaining a unitary power factor. This reference is also used to evaluate the tracking capabilities of control strategies, particularly under realistic operating conditions. Moreover, from a regulatory standpoint, standards such as IEEE 1547 and IEC 61727 mandate sinusoidal current injection with minimal distortion for distributed energy resources interfacing with public grids [22].

Thus, the model presented in (4) can be rewritten as follows:

$$\begin{bmatrix} L_s\dot{x}_1^\star \\ C_o\dot{x}_2^\star \\ L_g\dot{x}_3^\star \end{bmatrix} = \begin{bmatrix} -r_s & -u^\star & 0 \\ u^\star & 0 & -1 \\ 0 & 1 & -R_g \end{bmatrix} \begin{bmatrix} x_1^\star \\ x_2^\star \\ x_3^\star \end{bmatrix} + \begin{bmatrix} V_s \\ 0 \\ -v_g \end{bmatrix} \tag{5}$$

To facilitate controller design, a linearized model can be derived through a small-signal perturbation approach [23], wherein the state variables and input signals are expressed as the sum of their steady-state values and small perturbations.

$$x = x^\star + \tilde{x}$$
$$u = u^\star + \tilde{u} \tag{6}$$

where $\tilde{x}$ and $\tilde{u}$ represent small perturbations.

The selection of a sinusoidal current trajectory is relevant for the design of nonlinear controllers —including IDA-PBC, PI-PBC, and other passivity-based strategies— since these methods rely on accurately capturing the system's energy dynamics [24]. Through this dynamic representation, the next subsection will introduce the Hamiltonian model, which provides an energy-based perspective for analyzing system behavior and designing robust control strategies.

2.3. Hamiltonian model

The Hamiltonian modeling approach provides a framework for analyzing and controlling power electronic converters [25]. This formulation, rooted in the principles of energy shaping and passivity, is particularly suitable for the synthesis of PBC strategies such as IDA-PBC and PI-PBC [13, 26].

To derive the state-space representation of the PWM-CSC in Hamiltonian form, the System Dynamics (4) can be rewritten as shown in Equation (8).

$$\begin{bmatrix} L_s & 0 & 0 \\ 0 & C_o & 0 \\ 0 & 0 & L_g \end{bmatrix} \begin{bmatrix} \dot{x_1} \\ \dot{x_2} \\ \dot{x_3} \end{bmatrix} = \left(\begin{bmatrix} 0 & -u & 0 \\ u & 0 & 1 \\ 0 & -1 & 0 \end{bmatrix} - \begin{bmatrix} r_s & 0 & 0 \\ 0 & 0 & 0 \\ 0 & 0 & R_g \end{bmatrix} \right) \begin{bmatrix} x_1 \\ x_2 \\ x_3 \end{bmatrix} + \begin{bmatrix} V_s \\ 0 \\ -v_g \end{bmatrix} \tag{7}$$

$$\mathcal{D}\dot{x} = \left(\mathcal{J}\left(u\right) - \mathcal{R}\right) x + \vartheta, \tag{8}$$

Here, the vector x represents the system states in the Hamiltonian formulation; $\mathcal{D}$ is an energy storage or metric matrix that defines the system structure; $\mathcal{J}\left(u\right)$ is an interconnection structure matrix dependent on the control variable u, which determines the energy dynamics in the system and is skew-symmetric, meaning that $\mathcal{J}\left(u\right) + \mathcal{J}^\top\left(u\right) = 0$; $\mathcal{R}$ is a damping or dissipation matrix representing resistive effects and system losses; and ϑ is an external excitation term that may include voltage sources [27].

Moreover, $\mathcal{D}$ is a symmetric and positive-definite matrix that represents the system's storage elements. Specifically, it is a diagonal matrix $\mathcal{D} = \text{diag}(L_s, C_o, L_g)$ and corresponds to the inductive and capacitive components that accumulate energy in the form of magnetic and electric fields. This matrix defines the generalized momentum associated with each state [28].

The skew-symmetric matrix $\mathcal{J}(u)$ determines the power-conserving interconnection between state variables. It models how energy is redistributed among the system components without being dissipated. Its dependence on the control input u reflects the fact that modulation actively changes the energy exchange pathways. In addition, its skew-symmetry ensures that no energy is generated or lost in this process [29].

The dissipation matrix $\mathcal{R}$ is symmetric positive-semidefinite and models the energy losses of the system due to resistive components. It includes parameters such as r_s (the series resistance of L_s) and R_g (the load resistance) and ensures that the system reflects the physical reality of non-ideal components, where part of the energy is irreversibly dissipated [30].

The dynamical system expressed in (8) admits the equilibrium trajectory. Its corresponding dynamic behavior is described by the following equation:

$$\mathcal{D}\dot{x}^\star = \left(\mathcal{J}\left(u^\star\right) - \mathcal{R}\right) x^\star + \vartheta, \tag{9}$$

where $\dot{x}^\star$ represents the time derivative of the trajectory (which is nonzero for single-phase converter applications), and $u^\star$ represents a smooth control input.

To synthesize a controller under the PBC framework, it is necessary to derive an incremental model that captures the error dynamics of the system. To this effect, the state and input errors are defined in Equations (6). By subtracting the desired closed-loop dynamics from the open-loop system equations and performing some algebraic manipulations, the incremental model is obtained:

$$\mathcal{D}\dot{\tilde{x}} = \mathcal{J}(\tilde{u})x^\star + (\mathcal{J}(u) - \mathcal{R})\tilde{x}. \tag{10}$$

3. Control strategies

3.1. NPI control

NPI control is an extension of the classical PI controller that incorporates nonlinear compensation terms to improve the system's response under dynamic conditions [31]. Traditional PI controllers regulate the error signal by adjusting the proportional (P) and integral (I) gains, but they often struggle with highly dynamic loads and nonlinearities in power electronic systems.

An NPI controller introduces a state-dependent gain adaptation, allowing it to dynamically adjust its response based on the system's operating state [32]. This results in an improved transient response, a reduced steady-state error, and a better disturbance rejection.

The general NPI control law is expressed as follows:

$$\tilde{u} = -k_p\tilde{x}_2 - k_i\int \tilde{x}_2 dt \tag{11}$$

where k_p and k_i are positive constants that determine the proportional and integral actions, respectively. In addition, the term $\tilde{x}_2 = x_2 - x_2^\star$ represents the error between the system state and its desired reference, which is designed to asymptotically converge to zero.

$$u = \frac{1}{x_1^*}\left(C_o\dot{x}_2^\star + x_3^\star - k_p\tilde{x}_2 - k_i\int \tilde{x}_2 dt\right). \tag{12}$$

This control law ensures that the input u is dynamically adjusted based on the error signal and its integral, allowing the system to effectively track the reference trajectory.

To assess the stability of the closed-loop system under this control strategy, Lyapunov's stability theorem is applied. This theorem states that, if a positive-definite Lyapunov function $\mathcal{V}(x)$ can be found such that its time derivative $\dot{\mathcal{V}}(x)$ is negative-definite, then the equilibrium point of the system is globally asymptotically stable [33]. For the proposed NPI controller, this implies that the system states (x_1, x_2, x_3) converge to their desired values as $t \to \infty$, which ensures global asymptotic stability.

Figure 3 presents a comparison between the desired reference current i_g and the values obtained for the load of the PWM-CSC under the NPI control scheme. This plot shows that the obtained signal (green line) closely follows the imposed reference (purple line) after an initial adjustment period. The control parameters were set to $k_p = 0.008$ and $k_i = 0.005$, resulting in a suitable control signal that ensured proper system operation.

The behavior of the current i_s and the voltage across the capacitor v_c, corresponding to the other state variables, can be observed in Figures 4 and 5.

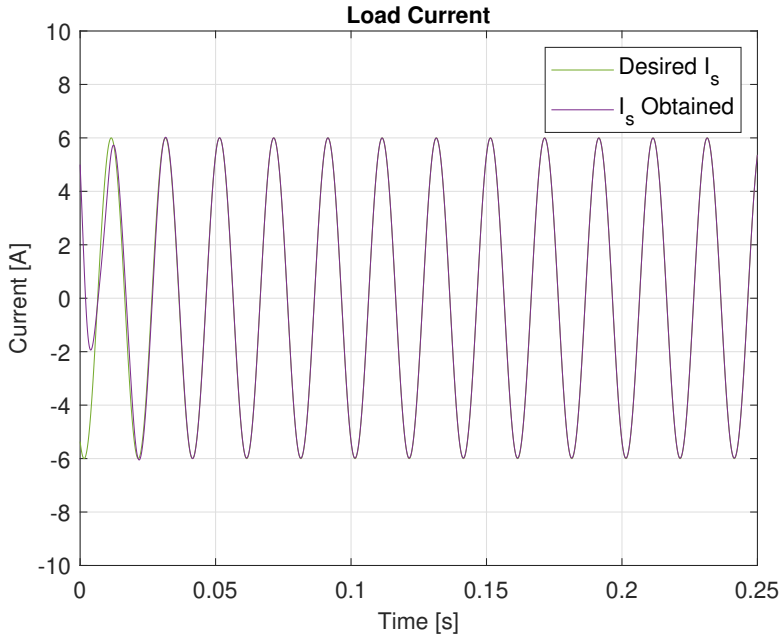

Figure 3. Tracking performance regarding load current under the NPI control strategy

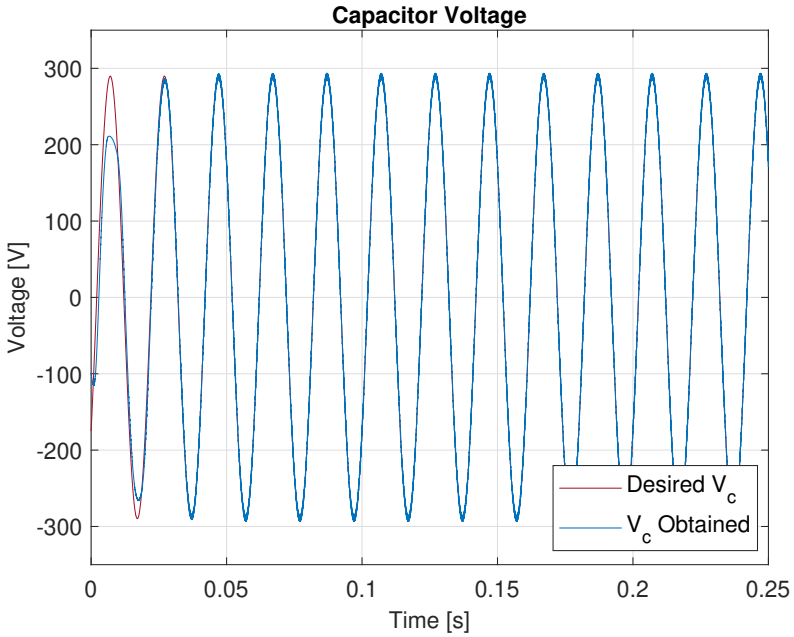

Figure 4. Tracking performance regarding capacitor voltage under the NPI control strategy

3.2. PI-PBC

PI-PBC is a robust approach that builds upon passivity theory to enhance system stability and improve tracking accuracy [34]. By introducing an additional integral term into the PBC framework, this method significantly

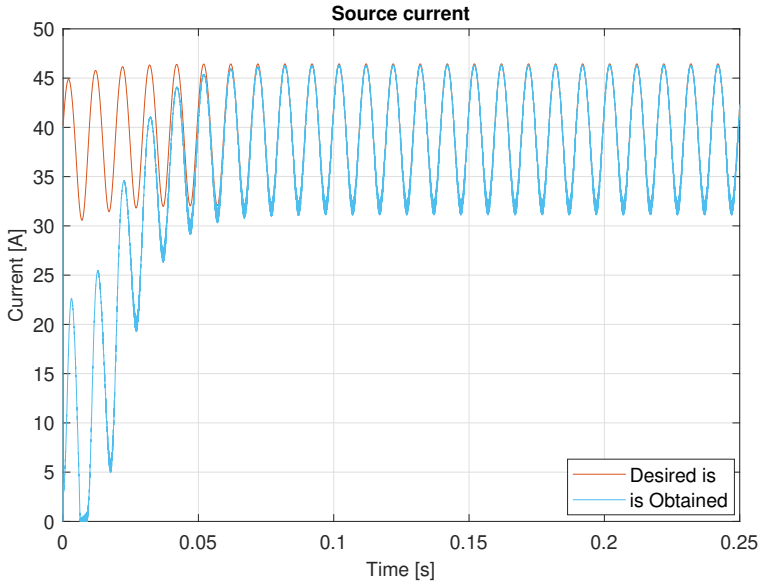

Figure 5. Tracking performance regarding the source current under the NPI control strategy

improves disturbance rejection while ensuring a zero steady-state error, even in the face of load variations [35]. PI-PBC merges the advantages of PBC with PI regulation, leading to improved state tracking, enhanced disturbance attenuation, and superior reference trajectory convergence [36]. This approach is particularly well-suited for dynamical systems modeled within the port-Hamiltonian framework, as it leverages the inherent energy properties of the system to ensure Lyapunov stability.

The incremental model described in Equation (10) can be asymptotically stabilized by implementing a suitable PI-based control law [37]. The proposed control law is designed to drive the system towards a stable equilibrium at $\tilde{x} = 0$, under the condition that the control input perturbation $\tilde{u} = 0$ is defined as follows:

$$\begin{aligned} \tilde{u} &= -k_p \tilde{y} - k_i \tilde{z}, \\ \dot{\tilde{z}} &= \tilde{y}, \end{aligned} \tag{13}$$

where k_p and k_i are positive control gains, and $\tilde{y}$ represents the system's passive output. This passive output is computed as follows:

$$\tilde{y} = x^{\star,\top} \mathcal{J}_1 \tilde{x} \tag{14}$$

$$= \begin{bmatrix} x_1^\star & x_2^\star & x_3^\star \end{bmatrix} \begin{bmatrix} 0 & -1 & 0 \\ 1 & 0 & 0 \\ 0 & 0 & 0 \end{bmatrix}^\top \begin{bmatrix} \tilde{x}_1 \\ \tilde{x}_2 \\ \tilde{x}_3 \end{bmatrix} \tag{15}$$

$$= x_1^\star \tilde{x}_2 - x_2^\star \tilde{x}_1. \tag{16}$$

Thus, the PI-PBC control law is given by

$$\tilde{u} = -k_p \left(x_1^\star \tilde{x}_2 - x_2^\star \tilde{x}_1 \right) - k_i \int \left(x_1^\star \tilde{x}_2 - x_2^\star \tilde{x}_1 \right) dt. \tag{17}$$

Considering that the total control input is defined as $u = u^\star + \tilde{u}$, and incorporating the expressions from Equations (3) and (17), the resulting control input equation is

$$u = \frac{1}{x_1^\star}\left(C_o \dot{x}_2^\star + x_3\right) - k_p\left(x_1^\star \tilde{x}_2 - x_2^\star \tilde{x}_1\right) - k_i \int \left(x_1^\star \tilde{x}_2 - x_2^\star \tilde{x}_1\right) dt. \tag{18}$$

To validate the asymptotic stability of the system under the proposed control strategy, a Lyapunov candidate function is selected as the Hamiltonian function.

$$\mathcal{V}\left(\tilde{x}, \tilde{z}\right) = \frac{1}{2}\tilde{x}^\top \mathcal{D}\tilde{x} + \frac{1}{2}\tilde{z}^\top k_i \tilde{z}, \tag{19}$$

which is positive-definite and satisfies $\mathcal{V}(0) = 0$. Evaluating the time derivative of this function yields the following:

$$\begin{aligned} \dot{\mathcal{V}}\left(\tilde{x}, \tilde{z}\right) &= \tilde{x}^\top \mathcal{D}\dot{\tilde{x}} + \tilde{z}^\top k_i \dot{\tilde{z}}, \\ &= \tilde{x}^\top \left(\mathcal{J}\left(\tilde{u}\right) x^\star + \left(\mathcal{J}\left(u\right) - \mathcal{R}\right)\tilde{x}\right) + k_i \tilde{z}\tilde{y} \\ &= -\tilde{x}^\top \mathcal{R}\tilde{x} - \tilde{y}^\top k_p \tilde{y} < 0. \end{aligned} \tag{20}$$

Since $\dot{\mathcal{V}}\left(\tilde{x}, \tilde{z}\right)$ is negative-definite, the system described by Equations (10) and (18) is asymptotically stable in the sense of Lyapunov. This implies that $x \to x^\star$ as $t \to \infty$, ensuring the convergence of the system to the desired equilibrium state.

Figure 6 illustrates the load current response under the PI-PBC controller with $k_p = 0.1e^{-3}$ and $k_i = 0.1e^{-3}$. Initially $(t < 0.05s)$, a noticeable transient error is observed, indicating a slow response in tracking the desired current. Then, however, the obtained current closely follows the reference, demonstrating that the controller effectively eliminates the steady-state error, which is likely due to the integral action. The controller ensures stability and accurate tracking in the steady state, but a more aggressive tuning could improve its dynamic response.

Figure 7 depicts the capacitor voltage response under the PI-PBC control strategy. The obtained voltage closely follows the desired reference, exhibiting a well-regulated sinusoidal waveform after a brief transient period. This indicates that the controller effectively stabilizes the system and enforces the desired dynamics.

Similarly, the input source current (Figure 8) exhibits a comparable behavior, tracking its reference signal with slight deviations. However, there is some noise in the current waveform, which may stem from measurement inaccuracies, switching effects, or unmodeled system dynamics. Despite this, the overall performance suggests that the controller maintains stability while ensuring a proper dynamic response.

3.3. IDA-PBC

IDA-PBC is a nonlinear control technique that exploits the properties of Hamiltonian systems and passivity theory [38]. The fundamental goal of this approach is to redesign the closed-loop dynamics in order to ensure system stability while preserving the intrinsic port-Hamiltonian structure [15]. To this effect, the system is restructured into the desired port-Hamiltonian form, as given by

$$\mathcal{D}\dot{\tilde{x}} = \mathcal{J}_d(u) - \mathcal{R}_d\tilde{x}, \tag{21}$$

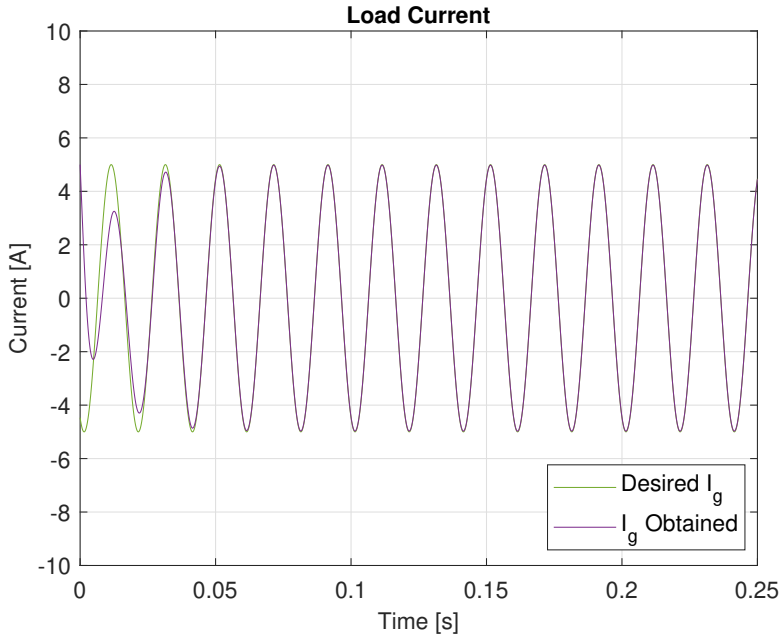

Figure 6. Tracking performance regarding load current under the PI-PBC

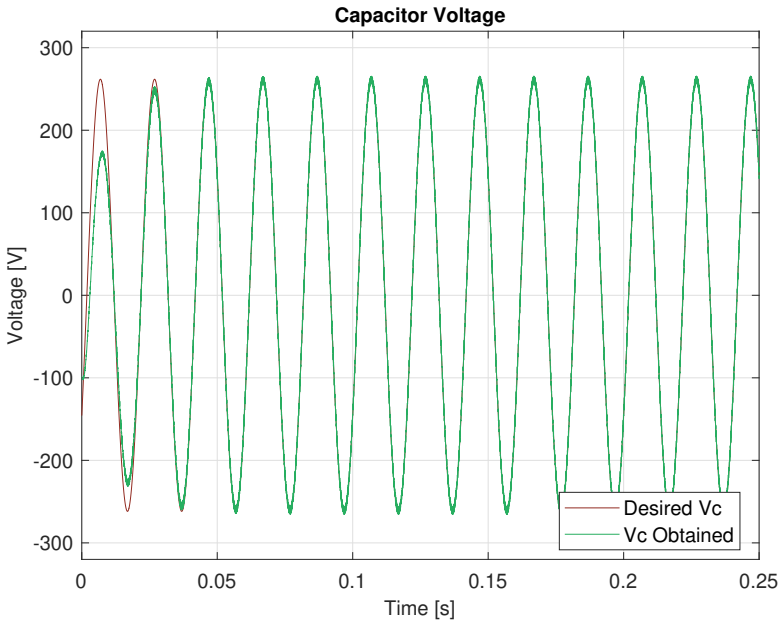

Figure 7. Tracking performance regarding capacitor voltage under the PI-PBC

where $\mathcal{J}_d$ and $\mathcal{R}_d$ denote the desired interconnection and dissipation matrices, respectively. These matrices must be designed such that R_d is positive-definite, ensuring energy dissipation. Meanwhile, J_d remains skew-symmetric, satisfying the condition $\mathcal{J}(u) + \mathcal{J}^\top(u) = 0$. This design effectively eliminates undesired open-loop

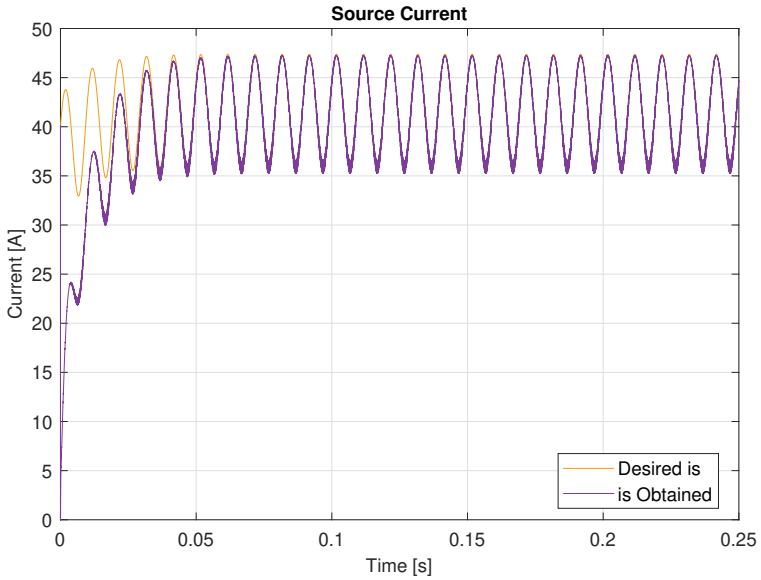

Figure 8. Tracking performance regarding the source current under the PI-PBC

interconnections and introduces sufficient damping to stabilize the system.

To derive the error dynamics of the system, the state variable errors are defined as $\tilde{x} = x - x^\star$ and $\tilde{u} = u - u^\star$. By subtracting the desired dynamical system from the open-loop system and performing some algebraic manipulations, the incremental error model is obtained:

$$\mathcal{D}\dot{\tilde{x}} = \mathcal{J}(\tilde{u})x^\star + (\mathcal{J}(u) - \mathcal{R})\tilde{x}. \tag{22}$$

The closed-loop control law is obtained by equating the Open-Loop System Dynamics (21) to the Desired Dynamics (22), yielding

$$\mathcal{J}(\tilde{u})x^\star + (\mathcal{J}(u) - \mathcal{R})\tilde{x} = (\mathcal{J}d - \mathcal{R}d)\tilde{x}, \tag{23}$$

$$\mathcal{J}(\tilde{u})x^\star = \mathcal{J}_1 - (\mathcal{R}d - \mathcal{R})\tilde{x}. \tag{24}$$

The solution to (24) depends on an appropriate selection of the desired interconnection matrix, the dissipation matrix, and the Hamiltonian function. Said matrices are defined as follows:

$$\mathcal{J}d = \mathcal{J}(u) + \mathcal{J}_1$$

where:

$$\mathcal{J}d = \begin{pmatrix} 0 & -\omega & 0 \\ \omega & 0 & 0 \\ 0 & 0 & 0 \end{pmatrix}, \quad \mathcal{R}d = \begin{pmatrix} R_1 & 0 & 0 \\ 0 & R_2 & 0 \\ 0 & 0 & R_3 \end{pmatrix}. \tag{25}$$

By solving Equation (24), the control law is obtained:

$$\tilde{u} = \left(g(x^\star)^\top g(x^\star)\right)^{-1} g(x^\star)^\top \left(\mathcal{J}1 - (\mathcal{R}d - \mathcal{R})\tilde{x}\right), \tag{26}$$

$$\tilde{u} = \frac{1}{x_1^\star + x_2^\star}\begin{pmatrix} -x_2^\star & x_1^\star & 0 \end{pmatrix}\left[\begin{pmatrix} 0 & -\omega & 0 \\ \omega & 0 & 0 \\ 0 & 0 & 0 \end{pmatrix} - \left(\begin{pmatrix} R_1 & 0 & 0 \\ 0 & R_2 & 0 \\ 0 & 0 & 0 \end{pmatrix} - \begin{pmatrix} r_s & 0 & 0 \\ 0 & 0 & 1 \\ 0 & -1 & R_g \end{pmatrix}\right)\begin{pmatrix} \tilde{x}_1 \\ \tilde{x}_2 \\ \tilde{x}_3 \end{pmatrix}\right] \tag{27}$$

where

$$g(x^\star) = \begin{pmatrix} -x_2^\star \\ x_1^\star \\ 0 \end{pmatrix}.$$

The total control input, combining the equilibrium and the incremental components, is expressed as shown in Equation (27).

By substituting $u = u^\star + \tilde{u}$, the complete control input is obtained:

$$u = \frac{1}{x_1^\star}\left(C_o \dot{x}_2^\star + x_3^\star\right) + \tilde{u} \tag{28}$$

To demonstrate the asymptotic stability of the closed-loop system, consider the following Lyapunov candidate function:

$$\mathcal{V}(\tilde{x}) = \frac{1}{2}\tilde{x}^\top \mathcal{D}\tilde{x}, \tag{29}$$

which satisfies $\mathcal{V} > 0$ and $\mathcal{V} = 0$. The time derivative of $\mathcal{V}$ is given by

$$\begin{aligned} \dot{\mathcal{V}}(\tilde{x}) &= \tilde{x}^\top \mathcal{D}\dot{\tilde{x}}, \\ &= \tilde{x}^\top \left(\mathcal{J}(u) + \mathcal{J}1 - \mathcal{R}d\right)\tilde{x}, \\ &= -\tilde{x}^\top \mathcal{R}_d \tilde{x} < 0. \end{aligned} \tag{30}$$

Since $\dot{\mathcal{V}}(\tilde{x})$, the closed-loop system is asymptotically stable in the sense of Lyapunov, ensuring that $x \to x^\star$ as $t \to \infty$.

Figure 9 presents the load current response under the IDA-PBC, as designed with the specified parameters. The obtained current (i_g) closely follows the desired reference, with a transient period at the beginning. After approximately 0.05 seconds, the response stabilizes and accurately tracks the sinusoidal reference.

Compared to PI-PBC, IDA-PBC appears to provide a well-regulated response with minimal steady-state error. The parameter selection ($R_1 = 2.3$, $R_2 = 0.3$, and $R = 3.3$) successfully enforces the desired current profile, ensuring stability and an appropriate dynamic response.

Figures 10 and 11 illustrate the behavior of the voltage capacitor and the current inductor at the input. Both variables exhibit a similar transient response, characterized by an initial deviation that rapidly stabilizes. In both cases, the obtained signals closely follow the desired reference, demonstrating the effectiveness of the implemented control strategy in regulating these voltages and ensuring a proper system performance.

3.4. Implementation and practical considerations

The control gains for each strategy were tuned in two stages. In the initial phase, the gains were selected in order to ensure a satisfactory tracking response of the state variable x_3 to the sinusoidal reference trajectory.

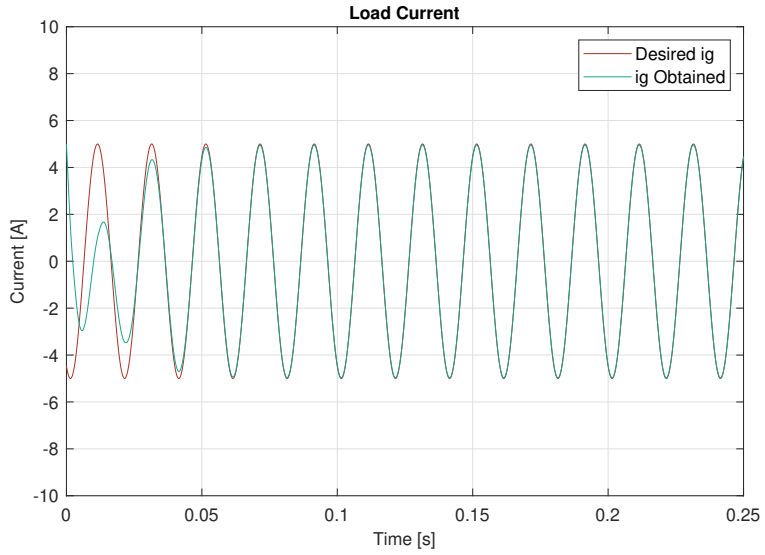

Figure 9. Tracking performance regarding load current under the IDA-PBC

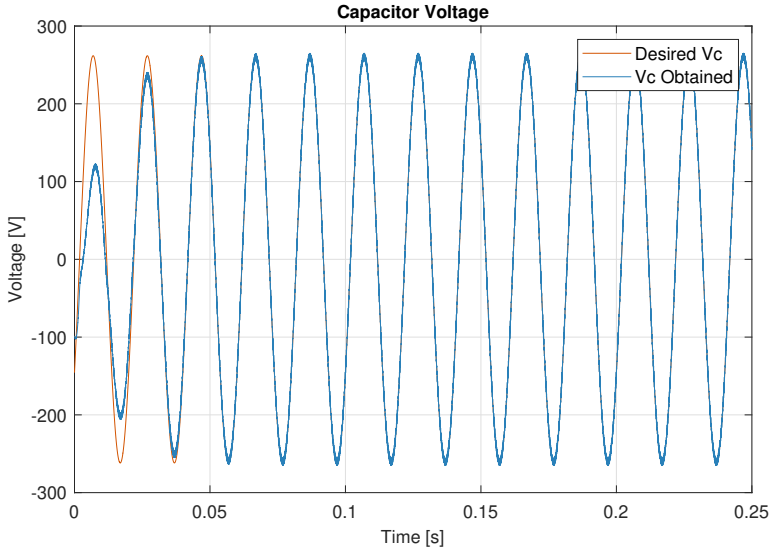

Figure 10. Tracking performance regarding capacitor voltage under the IDA-PBC

This preliminary step facilitated the identification of suitable regions for stable operation and accurate reference tracking.

Subsequently, fine-tuning was performed in order to adjust the controller parameters. The objective of this process was to improve the transient performance (*e.g.*, reduce the overshoot and settling time), ensure that the control signal $u(t)$ remained within the permissible range $[0, 1]$ (a requirement for modulation index constraints in PWM-based systems), and minimize the THD in the output current.

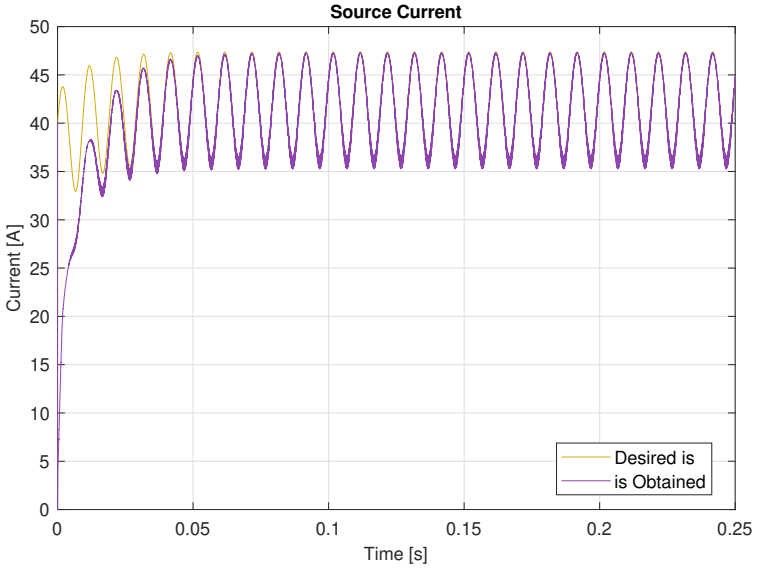

Figure 11. Tracking performance regarding the source current under the IDA-PBC

For the PI-PBC controller, the P and I gains k_p and k_i were increased incrementally, observing the impact on both the tracking error and the input modulation signal. In the case of IDA-PBC, the dissipative matrix $\mathcal{R}d$ was selected to satisfy the condition $\mathcal{R}d \succ 0$ (positive-definite), which ensures passivity and asymptotic stability.

The following step-by-step process was followed. The initial step involved introducing a modestly sized positive value for each R_i to ensure minimal damping and facilitate convergence. Here, it is imperative to augment R_1 in order to enhance the damping in the DC inductor loop (state x_1), R_2 must be adjusted to stabilize the capacitor dynamics (state x_2). To ensure fast and stable current tracking at the output (state x_3), it is necessary to tune R_3. This iterative approach enables the direct manipulation of the closed-loop energy dissipation, a process that is critical for ensuring the robustness and efficacy of IDA-PBC.

To enhance reproducibility, the control structure of each strategy was translated into modular algorithms. A detailed flowchart describing the implementation of the control laws and the generation of the reference trajectory is presented in Figure 2. This diagram outlines the control loop, initialization, real-time update of reference signals, and calculation of the modulation index.

The proposed control algorithms were designed with real-time deployment in mind. However, the following practical constraints must be considered for hardware implementation. First, the system was simulated with a sampling period of $T_s = 1\mu$ s. In hardware, the sampling rate must be at least ten times the highest frequency of interest to ensure accurate current control and modulation. Fixed-point representation and analog-to-digital conversion may introduce quantization noise, so careful scaling of the measured signals and the implementation of anti-windup mechanisms for the integral terms are essential. The output control signal $u(t)$, representing the modulation index, must remain within $[0, 1]$. The controllers were tuned to enforce this constraint dynamically, and saturation handling techniques were incorporated to prevent instability due to signal clipping.

4. Comparative analysis

To quantitatively compare the performance of the implemented control strategies, a set of standard performance indices widely cited in the literature [39–41] was employed. The following subsections present the selected indicators, their mathematical formulation, their interpretation, and the results obtained from simulation.

4.1. Integral of the squared error (ISE)

$$ISE = \int_0^T e^2(t)dt \tag{31}$$

where $e(t)$ denotes the error between the reference load current (i_g) and the measured load current. This index emphasizes large errors and provides a measure of the energy contained in the error signal [42].

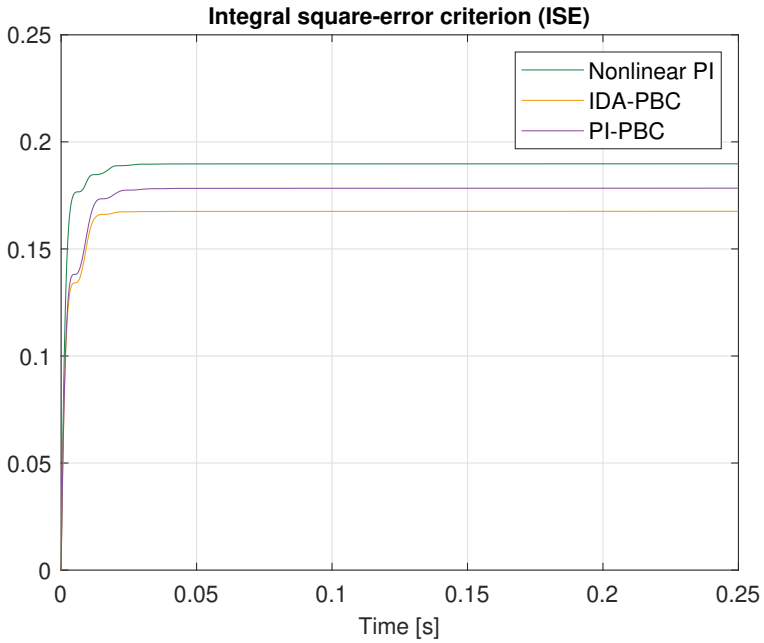

Figure 12. ISE comparison

Figure 12 shows the temporal evolution of the ISE for each controller. Note that the IDA-PBC achieves the lowest value, indicating a higher effectiveness in error suppression.

4.2. Integral of the time-weighted squared error (ITSE)

$$ISE = \int_0^T t \cdot e^2(t)dt \tag{32}$$

This index penalizes errors that persist over time, favoring strategies that rapidly eliminate deviations [43].

As shown in Figure 13, the NPI controller achieves the lowest value, suggesting a more efficient early-stage error reduction. The ITSE curve, like those of the IAE and ITAE, exhibits an increasing slope due to the cumulative nature of the error over time.

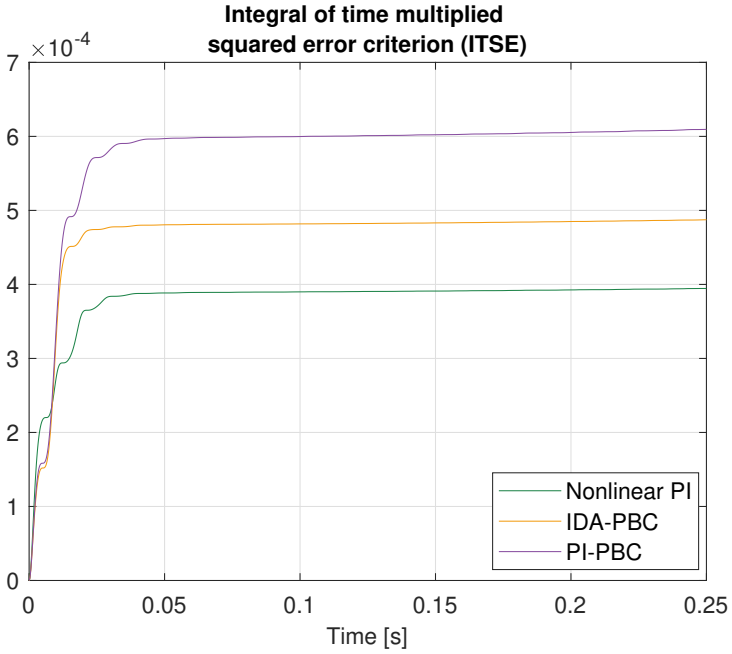

Figure 13. ITSE comparison

4.3. Integral of the absolute error (IAE)

$$IAE = \int_0^T |e(t)|\, dt \tag{33}$$

This metric evaluates the total magnitude of the error without emphasizing its duration or severity [44]. It provides an overall measure of the controller's error performance.

As shown in Figure 14, the error accumulates steadily over time. The NPI controller reaches the lowest value, although the performance gap between controllers is narrower compared to other indices.

4.4. Integral of the time-weighted absolute error (ITAE)

$$ITAE = \int_0^T t \cdot \left|e^2(t)\right| dt \tag{34}$$

This index penalizes sustained errors, making it especially useful to assess steady-state performance [45].

Figure 15 shows that the NPI controller reaches the lowest ITAE value, closely followed by IDA-PBC, suggesting that both strategies exhibit suitable dynamic and steady-state behavior.

4.5. Comparative analysis of the performance indices under study

Table 2 summarizes the final values of each performance indicator. The IDA-PBC exhibits the best performance in terms of ISE, while the NPI controller shows superior results for the ITSE, IAE, and ITAE. These findings suggest that IDA-PBC excels at reducing large errors, whereas NPI is more effective in achieving early and sustained error minimization.

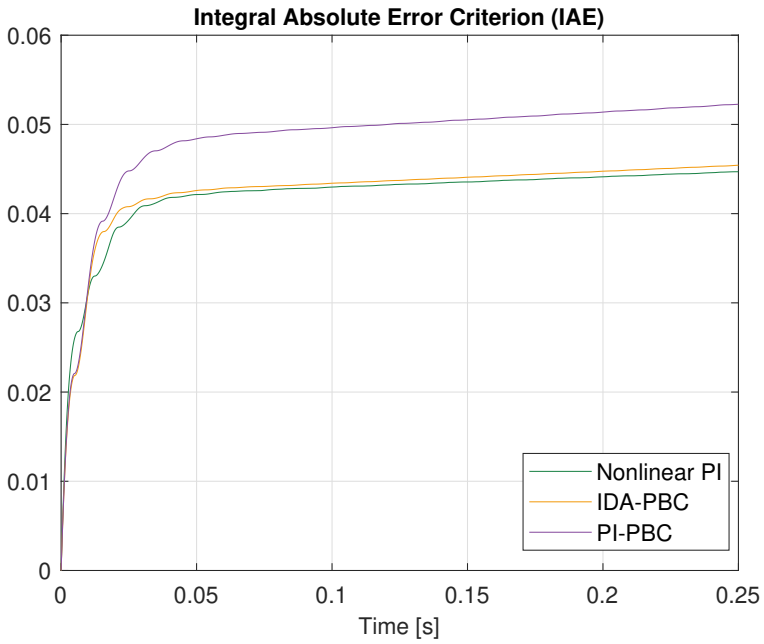

Figure 14. IAE comparison

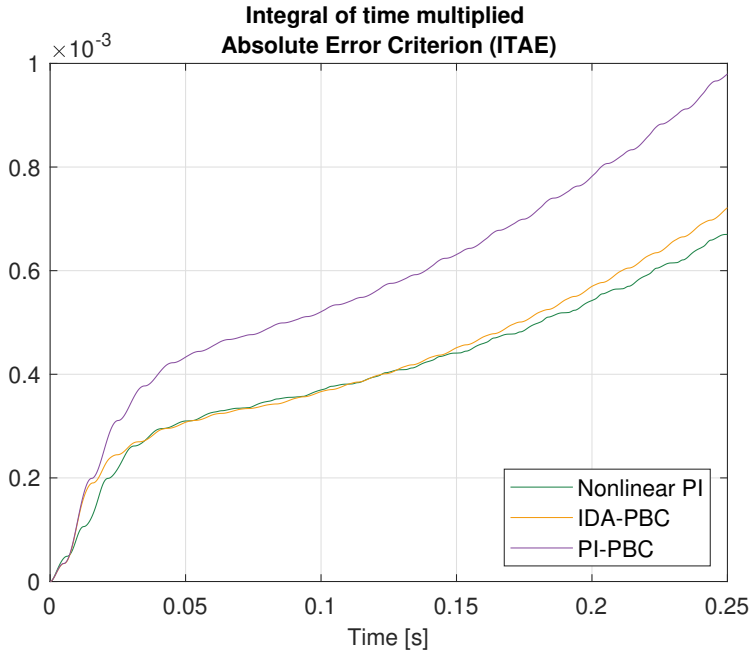

Figure 15. ITAE comparison

The IDA-PBC achieves the lowest ISE (0.1676), followed by PI-PBC (0.1783) and NPI (0.1897), suggesting its superior error minimization. As for the ITSE, the NPI controller performs better (3.94×10^{-4}), while PI-PBC reaches the highest value (6.082×10^{-4}), meaning that the former prioritizes error correction at earlier stages. In the case of the IAE, the differences are marginal, with NPI having the lowest (4.47×10^{-2}) and PI-PBC the

Table 2. Performance indices for each control strategy

Criterion	NPI	IDA-PBC	PI-PBC
ISE	0.1897	0.1676	0.1783
ITSE	3.94e-4	4.867e-4	6.082e-4
IAE	4.47e-2	4.541e-2	5.224e-2
ITAE	3.291e-4	3.243e-4	4.619e-4

highest value (5.224×10^{-2}). Finally, the ITAE follows a similar pattern, with NPI (3.291×10^{-4}) and IDA-PBC (3.243×10^{-4}) performing quite similarly. Meanwhile, PI-PBC reports the highest value (4.619×10^{-4}).

4.6. Total harmonic distortion (THD)

In addition to the performance indices, the THD in the current and voltage was evaluated, as shown in Table 3. The IDA-PBC achieved the lowest THD in current, which is advantageous for applications requiring high current quality. Conversely, the NPI controller yields the lowest voltage THD, making it suitable for scenarios where voltage quality is a priority.

Table 3. THD for each control strategy

THD(%)	NPI	IDA-PBC	PI-PBC
Current	0.182%	0.0615%	0.0864%
Voltage	1.375%	1.582%	1.585%

The IDA-PBC achieved the lowest THD in current (0.0615%), indicating a superior harmonic reduction compared to NPI (0.182%) and PI-PBC (0.0864%). However, in terms of voltage distortion, IDA-PBC and PI-PBC exhibited slightly higher values (1.582% and 1.585%, respectively) compared to the NPI controller (1.378%).

These findings suggest that IDA-PBC is the most effective strategy in reducing current harmonics, making it advantageous for applications where minimizing current distortion is a priority. Conversely, NPI shows the lowest voltage THD, which could be significant in systems where voltage quality is paramount. This comprehensive performance evaluation indicates that IDA-PBC yields superior results in terms of error minimization and current harmonic reduction, while NPI offers an advantage in terms of voltage quality.

The IDA-PBC exhibited the lowest THD in the output current, while the NPI controller achieved a lower THD in the output voltage. IDA-PBC was developed for shaping the energy of the system and enforcing a strict tracking of the current trajectory $x_3^\star$. Within this approach, the damping injection process, facilitated by the matrix $\mathcal{R}d$, is strategically designed to target the AC-side current loop. This targeted approach is intended to enhance the spectral purity of i_g and to minimize the THD.

However, this aggressive tracking can induce faster switching and sharp changes in the capacitor voltage v_c, especially under high damping, which slightly increases its spectral content. It has been demonstrated that, since the control voltage is not directly regulated but rather results from current injection, it is more susceptible to harmonic ripple under tightly constrained current tracking.

In contrast, the NPI method provides a smoother control action with a lower loop gain, allowing the voltage across the capacitor to settle more gradually, thus reducing its THD. However, this smoother behavior compromises current precision, leading to a slightly higher current THD.

This trade-off underscores a salient property of passivity-based methods: despite their intrinsic efficacy in shaping trajectories and enforcing the asymptotic convergence of energy-related states, the indirect management of non-dominant variables (*e.g.*, the voltage in the CSCs) can result in performance asymmetries [46]. Mitigation strategies may include coordinated voltage regulation, multi-objective control design, or composite controllers.

4.7. Limitations, robustness, and computational complexity

While the preceding sections have emphasized the merits of the suggested control strategies, it is imperative to recognize their practical limitations and trade-offs, particularly with regard to computational complexity, robustness to parameter uncertainty, and scalability to more intricate systems.

The implementation cost of the three strategies varies significantly. The NPI controller demonstrates a straightforward configuration, exclusively necessitating fundamental proportional and integral operations, *i.e.*, Equation (12). This simplicity makes it it well-suited for low-cost microcontrollers and real-time applications with tight computational constraints.

In contrast, PI-PBC and IDA-PBC require additional matrix computations. The PI-PBC formulation, shown in Equation (18), includes the computation of passive outputs and integral terms related to the system's energy interconnection. Concurrently, IDA-PBC introduces supplementary overhead through the design and implementation of interconnection and damping matrices, as shown in Equation (27). This necessitates matrix inversions and the symbolic manipulation of the skew-symmetric structure. Consequently, it may impose higher computational burdens, potentially requiring more capable embedded platforms (*e.g.*, DSPs or FPGAs) to ensure real-time feasibility.

In practical scenarios, the presence of component tolerances and environmental variations can introduce uncertainties in parameters such as the inductance L_s, the output capacitance C_o, and the grid-side impedance R_g. These variations can substantially affect the dynamic behavior and stability margins of CSCs. In order to evaluate the robustness of the proposed control strategies, a sensitivity analysis was conducted. In this analysis, L_s, L_g, and C_o were varied by $\pm 20\%$ with respect to their nominal values.

Figure 16 illustrates the current tracking performance of the three controllers under these parameter deviations. In each instance, the blue curve denotes the reference sinusoidal current, while the orange curve depicts the actual current injected by the converter under uncertain conditions.

The NPI controller exhibits an adequate tracking performance in the steady state. However, it reports significant phase lag and substantial transient deviations during the initial cycles. These effects are amplified under the simultaneous perturbation of both inductance and capacitance, confirming the controller's reduced robustness to model mismatches. The PI-PBC demonstrates superior disturbance rejection in comparison with the NPI controller. The result is improved phase alignment and reduced oscillation amplitude in early transients. However, this approach still exhibits mild overshoot and a longer convergence time when compared to IDA-PBC, which can be attributed to the absence of direct energy shaping mechanisms.

5. Conclusions and future works

This study presented a comparative analysis of three control strategies applied to PWM-CSCs operating in microgrids. The findings indicated that, while all three strategies achieved satisfactory current tracking performance under nominal conditions, IDA-PBC exhibited superior performance in terms of transient response, robustness to parameter variations, and THD minimization in the injected current.

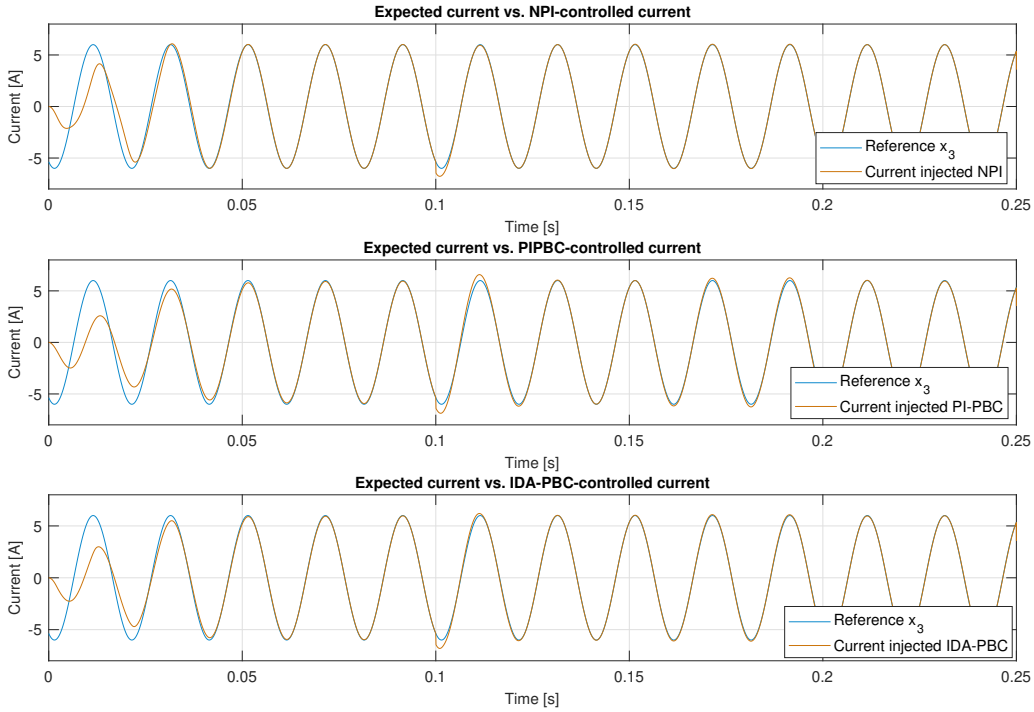

Figure 16. Tracking performance under parameter variations — Comparison between NPI, PI-PBC, and IDA-PBC

Note that the superior performance of IDA-PBC can be attributed to its ability to manipulate the energy configuration of the system and introduce artificial damping, thereby augmenting closed-loop stability, even in the presence of ± 20 percentage variations in inductance and capacitance. However, this enhanced performance is accompanied by an increase in computational complexity and a slight rise in voltage THD, attributable to the aggressive current tracking employed.

Experimental validation

While the conclusions drawn in this work are grounded in comprehensive simulation studies conducted in MATLAB/Simulink (version 2024b), a key limitation is the absence of an experimental validation. In future research, the proposed controllers will be implemented on real-time embedded hardware through a hardware-in-the-loop (HIL) testing framework. This platform will facilitate the verification of simulation results under real-world non-idealities such as sensor noise, IGBT switching losses, dead times, and a finite resolution from ADCs. The following aspects will be given particular attention:

- The effects of measurement noise and its mitigation through low-pass filtering and observer design
- Thermal variations in passive elements
- Saturation and delay effects in switching devices

This experimental stage will be pivotal in refining the controller design and validating its real-time feasibility.

Broader context and control strategy comparisons

Although this work focused on passivity-based methods and a NPI baseline, it is important to position the proposed strategies within the broader landscape of advanced control techniques. MPC and adaptive control are notable

alternatives that offer high performance in handling constraints and parameter uncertainties, respectively. However, these methods often imply higher computational costs and greater implementation complexity. The novelty of this study lies in applying energy-based passivity control to CSCs in single-phase systems with sinusoidal current injection, an area where direct comparative studies with PI-PBC and IDA-PBC are still scarce.

Future comparative studies will incorporate MPC and adaptive controllers to evaluate trade-offs in robustness, implementation complexity, and performance in dynamic and uncertain environments.

Extension to three-phase systems and fault conditions

An important direction for future research is the extension of these control strategies to three-phase PWM-CSCs, which introduces additional challenges such as unbalanced load conditions, inter-phase coupling dynamics, and zero-sequence current management.

Optimization for deployment

For practical deployment, future work will explore optimization strategies to reduce the computational burden without compromising control performance. These include lookup tables for nonlinear gain scheduling, reduced-order models of the converter for faster computation, precomputed damping matrices for IDA-PBC based on operating regimes, and hybrid control frameworks combining passivity-based methods with predictive or adaptive layers.

These enhancements will facilitate real-time implementation on low-power embedded platforms and will extend the applicability of the proposed methods to a wider range of energy conversion systems, including grid-forming converters in isolated or weak grids.

ACKNOWLEDGEMENTS

The authors express their sincere gratitude to the Doctoral Program in Engineering at Universidad Distrital Francisco José de Caldas for the support provided throughout this work. We also acknowledge the institutional backing of Universidad Distrital, which has facilitated the academic and technological resources essential for this research. This article represents a collective effort to advance knowledge in the field of power converter control, contributing meaningfully to the progress of electrical systems engineering.

The authors acknowledge the support provided by Thematic Network 723RT0150, titled *Red para la integración a gran escala de energías renovables en sistemas eléctricos (RIBIERSE-CYTED)*, funded by the 2022 call for Thematic Networks of the CYTED (Ibero-American Program of Science and Technology for Development).

REFERENCES

1. Zhongting Tang, Yongheng Yang, and Frede Blaabjerg. Power electronics: The enabling technology for renewable energy integration. *CSEE Journal of Power and Energy Systems*, 8:39–52, 1 2022.
2. Qiang Wei, Ling Xing, Dewei Xu, Bin Wu, and Navid R. Zargari. Modulation schemes for medium-voltage pwm current source converter-based drives: An overview. *IEEE Journal of Emerging and Selected Topics in Power Electronics*, 7(2):1152–1161, June 2019.
3. Amit Kumer Podder, Oishikha Chakraborty, Sayemul Islam, Nallapaneni Manoj Kumar, and Hassan Haes Alhelou. Control strategies of different hybrid energy storage systems for electric vehicles applications. *IEEE Access*, 9:51865–51895, 2021.
4. Yu Xue, Yongfeng Ren, Jinwei He, Hao Wang, and Hongjie Jia. Current Source Converter as an Effective Interface to Interconnect Microgrid and Main Grid. *Energies*, 15(17):6447, September 2022.
5. Christian Buzzio, Yamil S. Poloni, Germán G. Oggier, and Guillermo O. García. A current-source DC-AC converter and control strategy for grid-connected PV applications. *International Journal of Electrical Power &; Energy Systems*, 154:109399, December 2023.
6. Angélica Mercedes Nivia-Vargas, Oscar Danilo Montoya, and Walter Gil-González. Nonlinear Control Design for a Single-Phase PWM-CSC with an Adaptive Load Estimation. In *2024 IEEE Colombian Conference on Applications of Computational Intelligence (ColCACI)*, pages 1–6. IEEE, July 2024.

7. O D Montoya, O Acevedo, W Gil-González, M Holguín, and F M Serra. On the nonlinear control of a single-phase current source converter for sinusoidal voltage generation. *Journal of Physics: Conference Series*, 1448(1):012011, January 2020.
8. Shameem Ahmad, Saad Mekhilef, Hazlie Mokhlis, Mazaher Karimi, Alireza Pourdaryaei, Tofael Ahmed, Umme Kulsum Jhuma, and Suhail Afzal. Fuzzy logic-based direct power control method for pv inverter of grid-tied ac microgrid without phase-locked loop. *Electronics*, 10(24):3095, December 2021.
9. Sandip Kumar Das, Sarat Chandra Swain, Ritesh Dash, Jyotheeswara Reddy K, Dhanamjayalu C, Ravikumar Chinthaginjala, Ramakanta Jena, Hossam Kotb, and Ali ELrashidi. Design and analysis of upqc in a microgrid using model reference adaptive control ensemble with back-stepping controller. *Heliyon*, 10(14):e34140, July 2024.
10. Manuel Flota-Bañuelos, María Espinosa-Trujillo, José Cruz-Chan, and Tariq Kamal. Experimental study of an inverter control for reactive power compensation in a grid-connected solar photovoltaic system using sliding mode control. *Energies*, 16(2):853, January 2023.
11. Hussain Sarwar Khan, Muhammad Aamir, Kimmo Kauhaniemi, Mohsin Mumtaz, Muhammad Waqar Hassan, and Muhammad Ali. Improved finite control set model predictive control for distributed energy resource in islanded microgrid with fault-tolerance capability. *Engineering Science and Technology, an International Journal*, 24(3):694–705, June 2021.
12. Muhammad Maaruf, Sulaiman S. Ahmad, Waleed M. Hamanah, Abdullah M. Baraean, Md Shafiul Alam, Mohammad A. Abido, and Md Shafiullah. Advanced optimization methods for nonlinear backstepping controllers for quadrotor-slung load systems. *IEEE Access*, 13:66607–66621, 2025.
13. H. Komurcugil. Steady-State Analysis and Passivity-Based Control of Single-Phase PWM Current-Source Inverters. *IEEE Transactions on Industrial Electronics*, 57(3):1026–1030, March 2010.
14. Federico M. Serra, Lucas M. Fernández, Oscar D. Montoya, Walter Gil-González, and Jesus C. Hernández. Nonlinear voltage control for three-phase dc-ac converters in hybrid systems: An application of the pi-pbc method. *Electronics*, 9(5):847, May 2020.
15. Oscar Danilo Montoya, Federico M. Serra, and Gerardo Espinosa-Pérez. On the equivalence between pi-pbc and ioc designs: An application involving three-phase front-end converters. *IEEE Transactions on Circuits and Systems II: Express Briefs*, 71(1):241–245, January 2024.
16. Ruihang Bai, Biao Zhao, Tianji Zhou, Xueteng Tang, Jianguo Li, Bin Cui, Zhanqing Yu, and Rong Zeng. Pwm-current source converter based on igct-in-series for dc buck and constant-current application: Topology, design, and experiment. *IEEE Transactions on Industrial Electronics*, 70(5):4865–4874, May 2023.
17. Jiahang Xia, Xiaojiang Guo, Chenxin Wang, Xiaoling Xiong, Chengyong Zhao, and Chunyi Guo. Cooperative control strategy of fundamental frequency modulation-based current source converters for offshore wind farms. *IEEE Transactions on Power Delivery*, 37(6):4805–4815, December 2022.
18. Jiahui Jiang, Haoran Sun, and Huicui Wang. A comprehensive review of single-phase converter topologies with 2ω-ripple suppress. *Electrical Engineering*, 106(1):225–262, August 2023.
19. S. Vedith, J. N. Bhanu Tej, S. Sampath, M. Usha Sree, P. Nithin Rao, and K. Neelima. *Review on Pulse Width Modulation and Optimization Techniques for Multilevel Inverters*, pages 235–249. Springer Nature Singapore, 2022.
20. Dingteng Feng, Xiaoling Xiong, Xiaobo Li, Chenhao Yao, Chengyong Zhao, and Frede Blaabjerg. Improved phase control with two degrees of freedom for current source converter using in hvdc systems. *IEEE Transactions on Power Delivery*, 39(3):1512–1523, June 2024.
21. Ibrahim M. Alotaibi, Salim Ibrir, Mohammad A. Abido, and Muhammad Khalid. Nonlinear power system stabilizer design for small signal stability enhancement. *Arabian Journal for Science and Engineering*, 47(11):13893–13905, January 2022.
22. Marko A. Dimitrijević and Milutin Petronijević. The system for distributed energy resources testing according to the ieee 1547-2018 standard. *COMPEL - The international journal for computation and mathematics in electrical and electronic engineering*, 42:1021–1038, 11 2023.
23. Marc Cheah-Mane, Agusti Egea-Alvarez, Eduardo Prieto-Araujo, Hasan Mehrjerdi, Oriol Gomis-Bellmunt, and Lie Xu. Modeling and analysis approaches for small-signal stability assessment of power-electronic-dominated systems. *WIREs Energy and Environment*, 12(1), June 2022.
24. Maris Tõnso, Vadim Kaparin, and Juri Belikov. Port-hamiltonian framework in power systems domain: A survey. *Energy Reports*, 10:2918–2930, November 2023.
25. Methawin Jantra, Uthen Kamnarn, Burin Yodwong, Anon Namin, Charnyut Karnjanapiboon, Suchart Janjornmanit, Samart Yachiangkam, Pakawadee Wutthiwai, Krit Ratchapum, Ekkachai Chaidee, Surasak Yousawat, Teeruch Janjongcam, Suparak Srita, Pratch Piyawongwisal, Jedsada Yodwong, Noureddine Takorabet, and Phatiphat Thounthong. Design and modeling of a hamiltonian control law for a bidirectional converter in dc distribution applications. In *2023 IEEE Transportation Electrification Conference and Expo, Asia-Pacific (ITEC Asia-Pacific)*, pages 1–5. IEEE, November 2023.
26. Qing-Chang Zhong and Marcio Stefanello. Port-hamiltonian control of power electronic converters to achieve passivity. In *2017 IEEE 56th Annual Conference on Decision and Control (CDC)*, pages 5092–5097. IEEE, December 2017.
27. Harsh Sharma, Zhu Wang, and Boris Kramer. Hamiltonian operator inference: Physics-preserving learning of reduced-order models for canonical hamiltonian systems. *Physica D: Nonlinear Phenomena*, 431:133122, March 2022.
28. Dimitri Jeltsema and Arnau Dòria-Cerezo. Port-hamiltonian formulation of systems with memory. *Proceedings of the IEEE*, 100:1928–1937, 2012.
29. Gerardo Escobar, Arjan J. Van der Schaft, and Romeo Ortega. A hamiltonian viewpoint in the modeling of switching power converters. *Automatica*, 35:445–452, 3 1999.
30. Marco Cupelli, Sriram K. Gurumurthy, Siddharth K. Bhanderi, Zhiqing Yang, Philipp Joebges, Antonello Monti, and Rik W. De Doncker. Port controlled hamiltonian modeling and ida-pbc control of dual active bridge converters for dc microgrids. *IEEE Transactions on Industrial Electronics*, 66:9065–9075, 11 2019.
31. Yong Woo Jeong and Chung Choo Chung. Nonlinear proportional-integral disturbance observers for motion control of permanent magnet synchronous motors. *IEEE Control Systems Letters*, 6:3062–3067, 2022.
32. Abdullateef H. Bashiri. Empirical study of robust/developed pid control for nonlinear time-delayed dynamical system in discrete time domain. *Heliyon*, 10(9):e29749, May 2024.

33. M. Akbarian, N. Pariz, and A. Heydari. Constituting an extension of lyapunov's direct method. *SIAM Journal on Control and Optimization*, 62(4):2346–2366, August 2024.
34. Catalina González-Castaño, Antonio Véliz, Duberney Murillo-Yarce, Walter Gil-González, Carlos Restrepo, and Alejandro Garcés. Passivity-based control pi for the versatile buck-boost (vbb) converter. *IEEE Access*, 12:110394–110405, 2024.
35. Ming Li, Enjun Liu, Hua Geng, Yongtao Mao, Xing Wang, and Xing Zhang. Passivity-based control for the stability of grid-forming multi-inverter power stations. *IEEE Transactions on Industrial Electronics*, pages 1–11, 2025.
36. Oluleke Babayomi, Yu Li, Zhenbin Zhang, and Ki-Bum Park. Advanced control of grid-connected microgrids: Challenges, advances, and trends. *IEEE Transactions on Power Electronics*, 40(6):7681–7708, June 2025.
37. Walter Gil-González, Oscar Danilo Montoya, Sebastián Riffo, Carlos Restrepo, and Javier Muñoz. A global tracking sensorless adaptive pi-pbc design for output voltage regulation in a boost converter feeding a dc microgrid. *Energies*, 16(3):1106, January 2023.
38. Pablo Borja. Interconnection and damping assignment passivity-based control without partial differential equations. *2024 UKACC 14th International Conference on Control, CONTROL 2024*, pages 131–136, 2024.
39. Seyed Mohammad Hossein Mousakazemi. Comparison of the error-integral performance indexes in a ga-tuned pid controlling system of a pwr-type nuclear reactor point-kinetics model. *Progress in Nuclear Energy*, 132:103604, 2 2021.
40. Karim El Mezdi, Abdelmounime El Magri, and Lhoussain Bahatti. Advanced control and energy management algorithm for a multi-source microgrid incorporating renewable energy and electric vehicle integration. *Results in Engineering*, 23:102642, September 2024.
41. Dayarnab Baidya, Shreya Dhopte, and Mitradip Bhattacharjee. Sensing system assisted novel pid controller for efficient speed control of dc motors in electric vehicles. *IEEE Sensors Letters*, 7(1):1–4, January 2023.
42. Davut Izci, Serdar Ekinci, Emre Çelik, Mohit Bajaj, Vojtech Blazek, and Lukas Prokop. Dynamic load frequency control in power systems using a hybrid simulated annealing based quadratic interpolation optimizer. *Scientific Reports*, 14(1), October 2024.
43. Shreekanta Kumar Ojha and Maddela Chinna Obaiah. Optimization of a novel fopidn-(1+pidn) controller for renewable integrated multi-area load frequency control system with non-linearities. *IEEE Access*, 13:56736–56755, 2025.
44. Pablo Proaño, Marcelo Pozo, Carlos Gallardo, and Oscar Camacho. Non-linear pid control of ac current and dc voltage for a photovoltaic system operating on a microgrid. *Results in Control and Optimization*, 18:100514, March 2025.
45. Mateusz Pietrala, Piotr Leśniewski, and Andrzej Bartoszewicz. An itae optimal sliding mode controller for systems with control signal and velocity limitations. *Acta Mechanica et Automatica*, 17(2):230–238, April 2023.
46. Youssef Michel, Matteo Saveriano, and Dongheui Lee. A passivity-based approach for variable stiffness control with dynamical systems. *IEEE Transactions on Automation Science and Engineering*, 21:6265–6276, 2024.